Journal of Power Sources 191 (2009) 662–668

Contents lists available at ScienceDirect

Journal of Power Sources

journal homepage: www.elsevier.com/locate/jpowsour

Structure, morphology and electrochemical performance of Zn-doped $[Ni_4Al(OH)_{10}]OH$

Xiaorui Gao, Lixu Lei*, Meng Hu, Liwei Qin, Yueming Sun

School of Chemistry and Chemical Engineering, Southeast University, 2 Southeast University Road, Nanjing 211189, China

ARTICLE INFO

Article history:
Received 29 October 2008
Received in revised form 21 January 2009
Accepted 19 February 2009
Available online 4 March 2009

Keywords:
Layered double hydroxides
Electrochemical performance
Current density
Discharge capacity

ABSTRACT

A layered double hydroxide $[Ni_4Al(OH)_{10}]OH$ was doped with different amounts of Zn^{2+} by coprecipitation and subsequent hydrothermal treatment. The structures of the samples were investigated by XRD, which showed that all are layered double hydroxides with very similar lattice parameters; and samples treated hydrothermally have better crystallinity with ZnO phase. The ZnO exists in rods of several micrometers long, while the $[Ni_4Al(OH)_{10}]OH$ in disks of various sizes as shown in SEM images. It has been found that samples treated hydrothermally have higher discharge capacity and better cyclic stability, the maximum discharge capacities are 315 mAh g^{-1} and 300 mAh g^{-1} at discharge current densities of 400 mA g^{-1} and 2000 mA g^{-1}, respectively.

1. Introduction

β-$Ni(OH)_2$ has been used as the positive electrode material of commercial Ni/Cd, Ni/Zn and Ni/MH secondary alkaline batteries, and therefore received much attention from basic and applied researches [1–5]. It is well-known that the morphology (e.g. spherical [6–8] or lamellar [9]) of β-$Ni(OH)_2$ and additives (cobalt, calcium, zinc, or rare-earth-based oxides and hydroxides) [10–14] of the electrodes have profound effects on the performance of the electrode. Up to now, commercial β-$Ni(OH)_2$-based batteries gain great success in small facilities of low power output. However, when the batteries are used in the circumstance of high power input and output, it has been found that the battery performance is not as good as they are expected. For example, the cycle life and energy discharged are dramatically decreased. The problems may come from the facts that (1) $Ni(OH)_2$ is a poor electric conductor, therefore, some of the nickel hydroxide particle with poorer electric contact remains inactive while the electrode is charged or discharged at high rates and (2) normally, β-$Ni(OH)_2$ transforms into β-NiOOH upon oxidation or charging, however, the latter turns out to be γ-NiOOH when it is overcharged, which is very harmful to the cycle life because the volume of the electrode expands seriously. The expansion may lead to poor electric contact between the current collector and β-$Ni(OH)_2$/β-NiOOH, and subsequent decrease of discharge capacity of the battery. However, the fact is, for ultrafast charging, overcharges cannot be avoided.

β-$Ni(OH)_2$ has an polymorphic form, α-$Ni(OH)_2$, which is also electrochemically active. It can be oxidized to γ-NiOOH with only a small contraction of volume. Unlike β-NiOOH, the oxidation state of Ni in γ-NiOOH can be higher than +3, thus γ-NiOOH has higher energy density than β-NiOOH. Studies from various groups have revealed that α-$Ni(OH)_2$ has better performance in cycle life. The only problems found were that it is not stable in highly basic electrolyte, and it has lesser volumetric energy density.

By partial substitution of nickel in the nickel hydroxide lattice with other metal cations like Al^{3+}, a layered double hydroxide (LDH) is formed. The LDH can be expressed by a typical formula $[Ni_{1-x}M_x(OH)_2]^{x+}A_{x/n}^{n-}\cdot mH_2O$, where M is a trivalent cation or a mixture of trivalent and divalent cations. The structures of LDHs have been fully discussed in literatures [15–17]. Up to now, M in the formula that has been studied includes Co [18–20], Zn [21,22], Fe [23–25], Mn [25,26], Cr [25,26], V [27], besides Al [28–31]. It is highly stable to alkali, and it is still of high energy density [32–36]. For example, α-$Ni(OH)_2$ containing 20 mol% Al was found to be very stable in the aqueous solution of 6 mol L^{-1} KOH, and the specific capacity of discharge is 303 mAh g^{-1} at a charge–discharge rate of 0.33 C [36]. There was another report which found the discharge capacities of Ni/Al LDHs containing 10%, 20% and 30% were 320 mAh g^{-1}, 300 mAh g^{-1} and 284 mAh g^{-1}, respectively at the discharge rate of 0.3 C [33]. Recently, we have found that LDHs with an ideal formula of $[Ni_4Al(OH)_{10}]X\cdot mH_2O$ ($X = NO_3^-$ and OH^-) have marvellous performance when they are charged or discharged at high rates, can consequently be candidates for heavy duty batteries [37,38].

To benefit from the LDHs, one has to study them carefully under various conditions. As we all know, both electric and ionic

* Corresponding author. Tel.: +86 25 85686762; fax: +86 25 52090618.
E-mail address: lixu.lei@seu.edu.cn (L. Lei).

0378-7753/$ – see front matter © 2009 Elsevier B.V. All rights reserved.
doi:10.1016/j.jpowsour.2009.02.055

Table 1
Chemical composition of Zn-doped $[Ni_4Al(OH)_{10}]OH$ samples treated hydrothermally at 180 °C.

Samples, chemical formula	Ni (wt.%) found (calc.)	Al (wt.%) found (calc.)	Zn (wt.%) found (calc.)
$[Ni_4Al(OH)_{10}]OH$, $[Ni_{3.9}Al(OH)_{9.8}]OH{\cdot}5.5H_2O$	42.8 (42.5)	5.00 (5.01)	–
1, $[Ni_{3.65}Al(OH)_{9.3}]OH{\cdot}6H_2O{\cdot}0.48ZnO$	37.9 (38.0)	4.77 (4.79)	5.51 (5.57)
2, $[Ni_{3.7}Al(OH)_{9.4}]OH{\cdot}6H_2O{\cdot}0.95ZnO$	35.6 (35.8)	4.42 (4.45)	10.2 (10.2)
3, $[Ni_{3.8}Al(OH)_{9.6}]OH{\cdot}5.5H_2O{\cdot}1.58ZnO$	33.9 (33.9)	4.11 (4.10)	15.7 (15.7)

conductivity of the materials have serious impacts on their electrochemical performance, because the electrode reaction of nickel-based LDH is controlled by both. For example, different additives (e.g. Ni, Co, CoO, graphite powders) for enhancing electric contact between current collector and the active material can lead to very different electrochemical performance. We have also reported that interlayer anions in the LDH have profound effects on the electrochemical performance of $[Ni_4Al(OH)_{10}]X{\cdot}mH_2O$ ($X = NO_3^-$ and OH^-) [37].

In literature, it has been reported that introducing cations such as Zn^{2+} and Co^{2+} into the Ni/Al LDHs layers can improve the electric conductivity of the materials [18–21]. It is also known that crystallinity or morphology of the active materials has important impact on their electrochemical properties [32,33,38]. By hydrothermal treatment, better crystallinity, bigger tap density and higher discharge capacity can be obtained [39]. In this paper, we would like to investigate if they are still working in our new LDH electrode. Our Zn-doped $[Ni_4Al(OH)_{10}]OH$ samples were prepared by coprecipitation and subsequent hydrothermal treatment. The effects of hydrothermal temperature and doped Zn content on their structures, morphology and electrochemical properties were investigated.

2. Experimental

All chemicals used in this research were analytical grade reagents and used without further treatments. Distilled water used in the experiments was boiled for 30 min to remove any dissolved gases.

2.1. Preparation of Zn-doped $[Ni_4Al(OH)_{10}]OH$

All the samples were prepared by coprecipitation, hydrothermal treatment and anion exchange process similar to our previous report [38]. Under a N_2 flow and vigorous stirring, a solution of 1 mol L^{-1} NaOH was added into 100 mL of aqueous solution containing 40 mmol of $Ni(NO_3)_2$, 10 mmol of $Al(NO_3)_3$ and 10 mmol of $Zn(NO_3)_2$ solution until the pH value of the solution reached 7. After the resulted suspension was stirred for 10 h at 100 °C, it was transferred into a Teflon-lined autoclave, and the latter was placed and had been kept in an oven maintained at constant temperature for 1 day. The suspension was then filtered and washed with distilled water for three times. The solid product was transferred into a flask, and into the flask 30 mL of 1 mol L^{-1} NaOH solution was added. After the reaction mixture was stirred for another 8 h, it was filtered, washed and dried in vacuum at 60 °C. Three samples with different amounts (5, 10 and 15 mmol) of $Zn(NO_3)_2$ were synthesized, they are denoted as samples **1**, **2** and **3** hereafter respectively.

2.2. Characterizations of samples

The structures of samples were determined by X-ray diffraction (XRD) using a Rigaku D/max 2000/PC diffractometer with Cu Kα radiation ($\lambda = 1.5406$ Å, scan rate 0.02° s^{-1}). Peaks of the XRD spectra were fitted with program Xfit (http://www.ccp14.ac.uk/tutorial/xfit-95/xfit.htm) to find the full width at half maximum (FWHM) and the diffraction angles (2θ) of the refractions. The Scherrer equation and the Chekcell software were respectively used to calculate the particle sizes and cell parameters of samples. Metal content was determined by the analytical service at Nanjing University by using a Jarrel-Ash J-A1100 inductively coupled plasma (ICP) spectrometer. The morphology of the materials was observed using a LEO 1530VP scanning electron microscope (SEM) equipped with an energy dispersive X-ray spectrometer (EDS) System EDAX Genesis X-ray analyser.

2.3. Preparation of electrodes

A paste was prepared by mixing 50 mg of Zn-doped $[Ni_4Al(OH)_{10}]OH$ power with 160 mg of Ni powder, 40 mg of cobalt powder, appropriate amounts of polytetrafluoroethylene (PTFE) and carboxymethyl cellulose (CMC) suspension. The paste was

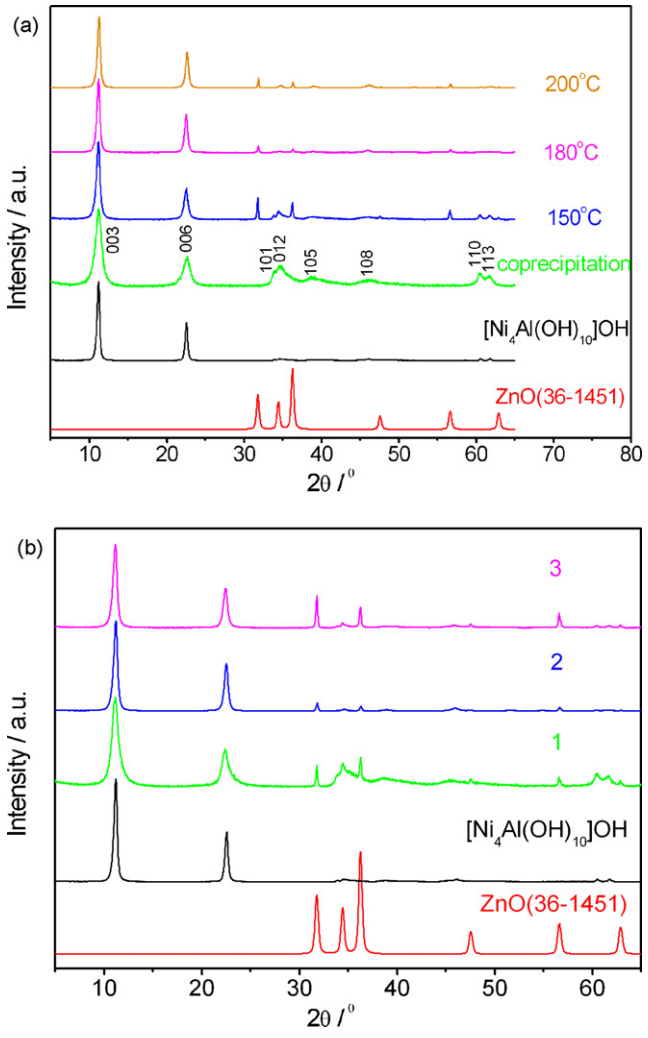

Fig. 1. XRD patterns of (a) sample **2** (coprecipiation), together with sample **2** treated hydrothermally at 150, 180 and 200 °C, respectively and (b) samples **1**, **2** and **3** treated hydrothermally at 180 °C.

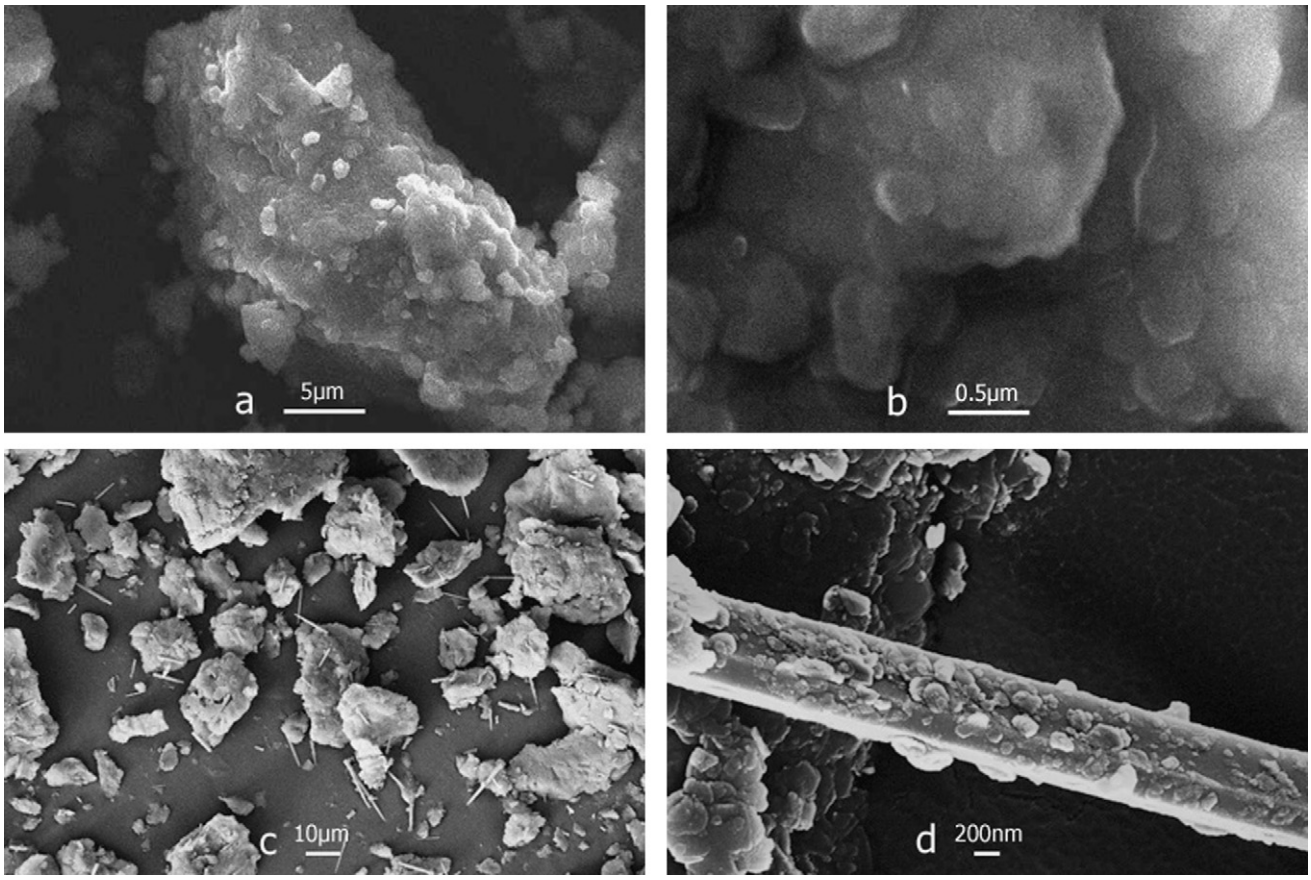

Fig. 2. SEM images of sample **2** synthesized by coprecipitation (a and b) and hydrothermal treatment at 180 °C (c and d).

incorporated into a nickel foam (Ø15 mm) using a spatula, dried at 80 °C for 24 h, and then pressed at 20 MPa to assure good electrical contact between the substrate and the active materials.

2.4. Electrochemical characterizations

Electrochemical characterizations were performed in a three-compartment electrolysis cell, in which a piece of Ni foam was used as the counter electrode and an Hg/HgO electrode as the reference electrode. Cyclic voltammetric studies were carried out on a CHI 660b electrochemical workstation at room temperature under an Ar flow. Galvanostatic charge–discharge studies were conducted on a LAND CT2001A cell performance tester. After the working electrode had been immersed in a 7-mol L^{-1} KOH for 24 h, it was charged at a current density of 100 mA g^{-1} for 4 h, and then discharged to 0 V vs. Hg/HgO at the same current density for activation. Such five cycles were done before further electrochemical characterization. The current densities, discharge capacities in the context of this paper were all calculated according to the actual mass of Zn-doped $[Ni_4Al(OH)_{10}]OH$ used in the electrode preparations.

3. Results and discussion

3.1. Structural and morphological characterizations

Table 1 gives the metal contents of as-prepared $[Ni_4Al(OH)_{10}]OH$ samples doped with different amounts of Zn and treated hydrothermally at 180 °C, the simulated formulas are also shown in it. It can be seen that the molar ratio of Ni to Al in the latter three samples is from 3.6 to 3.8, which is little smaller than that of $[Ni_4Al(OH)_{10}]OH$ sample. The possible reason is that part of Ni ions is substituted by Zn ions, which leads to the decrease of the content of Ni.

Fig. 1a shows the XRD patterns of sample **2**, together with sample **2** treated hydrothermally at 150, 180 and 200 °C. Fig. 1b shows the XRD patterns of samples **1**, **2**, and **3** treated hydrothermally at 180 °C. It can be seen that the XRD pattern of sample **2** without hydrothermal treatment is very similar to that of $[Ni_4Al(OH)_{10}]OH$ but the relative intensities and peak width at half maximum of the diffraction peaks. It can be seen that the sample **2** without hydrothermal treatment has poorer crystallinity. After hydrothermal treatment, the crystallinity of all samples becomes better, and peaks of ZnO appear.

An analysis of the XRD data in Fig. 1a is shown in Table 2, in which particle sizes are calculated by the Scherrer equation according to the strongest peak. Obviously, the particle size increases as the temperature of aging increases, which is in accordance with previous reports [38]. Peaks in the XRD patterns in Fig. 1 can be indexed on hexagonal cells of space group either *P*6222 or *P*63*CM*. The *P*6222 is one of the common space groups of layered double hydroxides

Table 2
XRD data and calculated partical sizes of sample **2** (coprecipitation, 100 °C), together with sample **2** treated hydrothermally at 150, 180 and 200 °C.

Temperature (°C)	FWHM (°)	2θ (°)	*d*-Value (nm)	Partical size (nm)[a]
100	1.0238	11.20	0.790	7.71
150	0.6021	11.16	0.793	13.1
180	0.5061	11.19	0.790	15.6
200	0.4704	11.25	0.786	16.8

[a] Particle sizes were calculated by using the Scherrer equation, $D = K\lambda/\beta\cos\theta$ where $K = 0.89$, D is the particle size, $\lambda = 0.15406$ nm, β is the FWHM in radians and θ is the Bragg angle of the reflection.

Table 3
The cell parameters of different amounts of Zn^{2+}-doped $[Ni_4Al(OH)_{10}]OH$ samples treated hydrothermally at 180 °C.

Samples	$[Ni_4AlZn_x(OH)_{10+2x}]OH$ (space group: *P*6222)		ZnO (space group: *P*63*CM*)	
	a (Å)	*c* (Å)	*a* (Å)	*c* (Å)
$[Ni_4Al(OH)_{10}]OH$	3.058	23.62	–	–
1	3.060	23.78	3.250	10.41
2	3.064	23.70	3.248	10.41
3	3.062	23.76	3.251	10.41

and *P*63*CM* is that of ZnO (JCPDS 36-1451). The lattice parameters are shown in Table 3.

It can be seen in Table 3 that the lattice parameters of the LDH phases with different amounts of Zn are very similar, but there are still small increases of both *a* and *c* for the Zn-containing samples, compared with the Zn-free sample. Because the radius of Zn^{2+} (0.74 Å) is larger than that of Ni^{2+} (0.70 Å), the substitution of Ni^{2+} by Zn^{2+} may result in the expansion of *a*-axis and *c*-axis. Therefore, we denote the LDH phase as $[Ni_4AlZn_x(OH)_{10+2x}]OH$ hereafter. However, we do not know how much is the value of *x* due difficulty to remove the ZnO phase only from the mixture.

The fact that ZnO or $Zn(OH)_2$ phase cannot be identified in the sample **2** without hydrothermal treatment is because that the ZnO or $Zn(OH)_2$ phase may be amorphous and in small amount. When the sample is treated hydrothermally, $Zn(OH)_2$ dehydrates to form ZnO and crystallize consequently [40–42]. The lattice parameters for ZnO in all samples are basically the same, therefore, ZnO exists in a sole phase.

Fig. 2 shows the SEM images of coprecipitated sample **2** without hydrothermal treatment and with hydrothermal treatment at 180 °C. It can be seen that the coprecipitated sample **2** without hydrothermal treatment is composed of irregular particles of tens of micrometers, which are actually formed from agglomeration of much smaller particles of disk-like grains (Fig. 2a and b); however, the sample contains some needle-like grains (Ø0.7 μm × 20 μm) after hydrothermal treatment (Fig. 2c and d). EDS analyses (Fig. 3) of the grains show that disk-like grains contain Ni, Al, Zn, while the needle-like ones contain only Zn and O. Therefore, the former is $[Ni_4AlZn_x(OH)_{10+2x}]OH$, the latter is ZnO. This is in accordance with the XRD studies.

Therefore, we conclude here that all the three Zn-doped samples have separate needle-like ZnO phase, and Zn also replaces some of Ni^{2+} in the lattice of $[Ni_4Al(OH)_{10}]OH$.

3.2. Electrochemical characterizations

3.2.1. Electrochemical properties of sample **2** treated hydrothermally at different temperatures

Fig. 4 shows the cyclic performance of sample **2** treated under different conditions. It can be seen that hydrothermal treatment can improve its cyclic performance. However, it seems that the discharge capacity of the sample treated at 200 °C drops very quickly compared with other samples. This is in accordance with a previous observation [38].

According to the structure of layered double hydroxides, the oxidation/reduction of them must involve intercalation/deintercalation of anions and water molecules, and the speed of intercalation/deintercalation determines its electrochemical performance. As we suggested before, we believe that regular structure can make interlayer anions move faster because the anions encounter less random scattering; and that less random scattering can also make the structure last longer [38]. Moreover, smaller particles means more grains in the same amount of active material, which makes less possible to have direct contact with the conductive additives, consequently less possibly be charged directly. In another word, if the particle of active material is too small, some of them cannot be charged rapidly, and therefore the material discharges less capacity. Therefore, the sample without hydrothermal treatment behaves the worst, and as the hydrothermal temperature increases, which means larger particles to be produced, the discharge capacity increases.

On the other hand, if the particle is too big, the diffusion distance of anions in the interlayer space would be long, which can also limit the speed of charging and consequent the discharge capacity. The fact that disk of large aspect ratio is easier to be broken also means that kind of material has shorter cycle life. That may give a clue why the sample treated at 200 °C give the worst cycle stability.

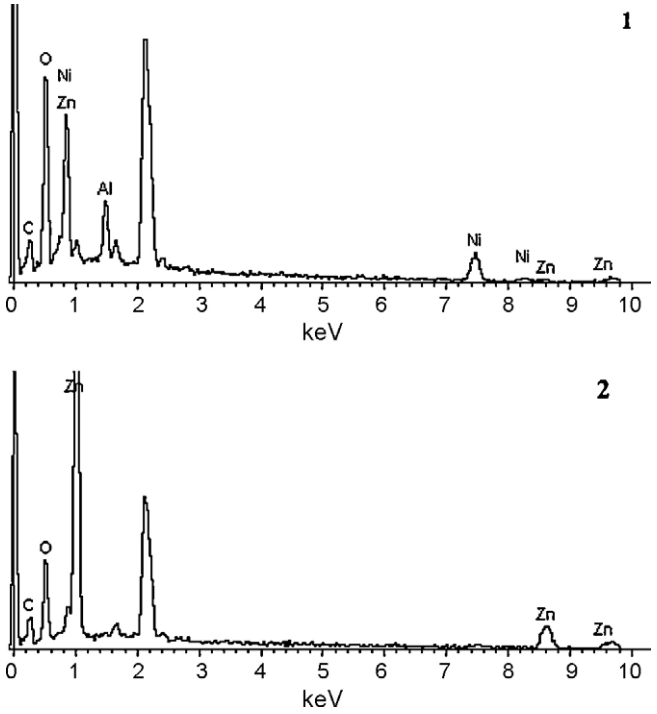

Fig. 3. EDS spectra of sample **2** synthesized by hydrothermal treatment at 180 °C (1: disk-like grains; 2: needle-like grains).

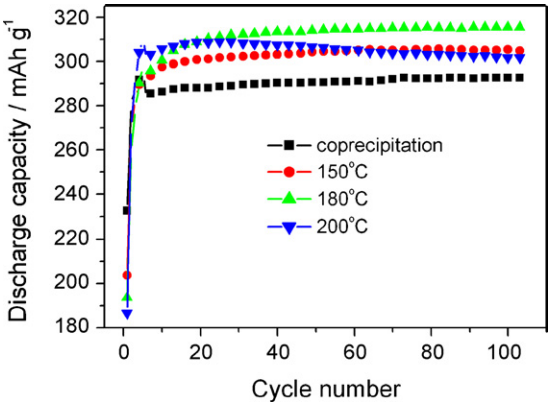

Fig. 4. Cyclic performance of electrode with sample **2** treated at different temperatures. In the initial five cycles, each cycle includes a charge at 5 mA (100 mA g^{-1}) and a discharge at 5 mA (100 mA g^{-1}). In the following 100 cycles, each cycle includes a charge at 40 mA (800 mA g^{-1}) and a discharge at 20 mA (400 mA g^{-1}).

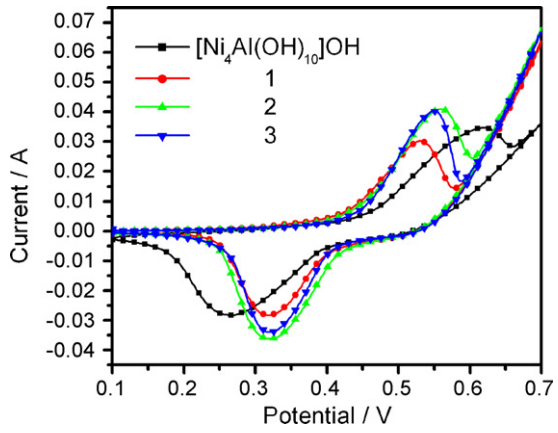

Fig. 5. Cyclic voltammograms of Zn-doped $[Ni_4Al(OH)_{10}]OH$ samples treated hydrothermally at 180 °C at the scan rate of 0.1 mV s^{-1} (in samples **1**, **2** and **3**, the doping amount of Zn is 5, 10 and 15 mmol, respectively).

3.2.2. *Electrochemical properties of $[Ni_4Al(OH)_{10}]OH$ doped with different amounts of Zn*

Fig. 5 gives the cyclic voltammograms of $[Ni_4Al(OH)_{10}]OH$ doped with different amounts of Zn at the scanning rate of 0.1 mV s^{-1} after 20 charge–discharge cycles (the charge current density is 800 mA g^{-1} and the discharge current density is 400 mA g^{-1}). It can be seen that the Zn-doped materials have smaller $\Delta E_{a,c}$ and the reductive peaks are almost at the same position for all of them. Because the oxidative peak appears significantly lower potentials than that of $[Ni_4Al(OH)_{10}]OH$ with no Zn, the Zn-doped materials can be charged at lower potentials without causing the evolution of oxygen. This may lead to more efficient charging, hence higher energy transformation efficiency.

The 28th discharge curves of $[Ni_4Al(OH)_{10}]OH$ samples doped with different amounts of Zn are shown in Fig. 6. It can be seen that only one discharge plateau is observed for all the samples, indicating that only one redox system is involved in the electrochemical reaction [34]. The discharge plateau of all electrodes is about 0.38 V (vs. Hg/HgO), which is higher than that of the β-$Ni(OH)_2$ electrode. This could be attributed to the large quantity of water molecules within the interlayer space of the Zn-doped $[Ni_4Al(OH)_{10}]OH$ samples, which is favorable to the proton diffusion during charge–discharge process [33]. Due to the inertness of Zn in electrochemical reaction, the discharge capacity should generally decrease as the increase of Zn content. However, the fact is not so straight, as it is found that sample **2** shows the highest discharge capacity. The possible reason might be that ZnO is a semiconductor [40–42], thus it is possible that ZnO increases the electronic conductivity of the samples, which leads to the increase of discharge capacity. As we have observed in Fig. 2, there are many ZnO rods in the sample.

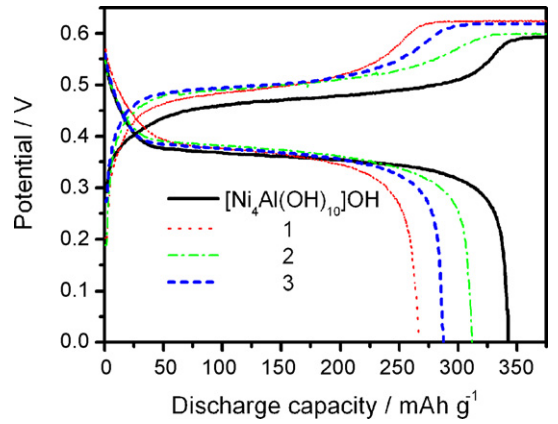

Fig. 6. The 28th discharge curves of Zn-doped $[Ni_4Al(OH)_{10}]OH$ samples treated hydrothermally at 180 °C (the charge current density is 800 mA g^{-1} and the discharge current density is 400 mA g^{-1}).

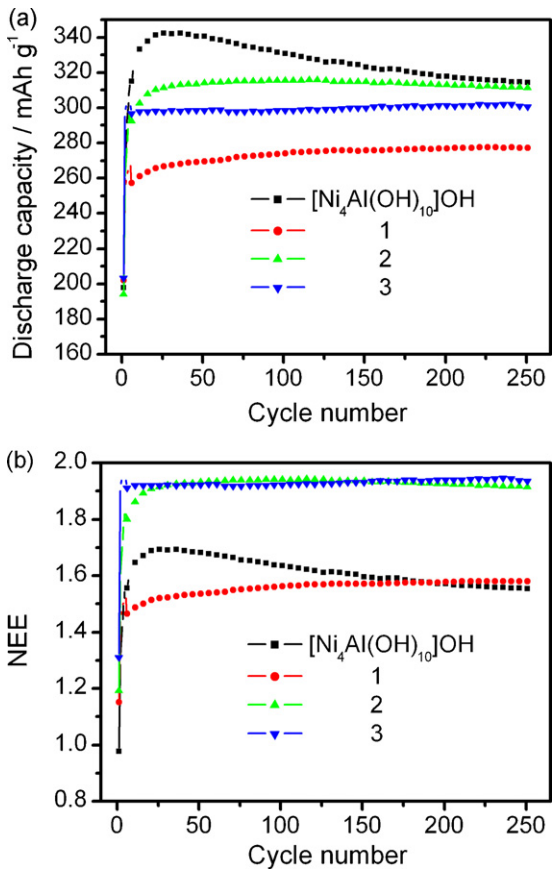

Fig. 7. (a) Gravimetric discharge capacity and (b) number of exchange electrons (NEE) as function of cycle number for electrodes made of Zn-doped $[Ni_4Al(OH)_{10}]OH$ samples treated hydrothermally at 180 °C. In the initial 5 cycles, each cycle includes a charge at 5 mA (100 mA g^{-1}) and a discharge at 5 mA (100 mA g^{-1}). In the following 250 cycles, each cycle includes a charge at 40 mA (800 mA g^{-1}) and a discharge at 20 mA (400 mA g^{-1}).

Gravimetric discharge capacities are given as functions of cycle number in Fig. 7a and the NEE analyses of the same data are shown in Fig. 7b. The $[Ni_4Al(OH)_{10}]OH$ sample exhibits the highest discharge capacity 343 mAh g^{-1}, which takes place in the initial stage of electrochemical cycle. However, after the 25th cycle the discharge capacity decreases quickly. At 255th cycle, discharge capacity attains 314 mAh g^{-1} and its deterioration rate is 8%. Contrastively, Zn-doped $[Ni_4Al(OH)_{10}]OH$ improves the charge–discharge cycle stability. The maximum discharge capacity of sample **2** is 315 mAh g^{-1}, and the deterioration rate is comparatively low, only 1% at 255th cycle. The significant improvement of Zn on the cycle stability of $[Ni_4Al(OH)_{10}]OH$ may be attributed to the fact that more micro-pores in favor of the penetration of electrolyte in the crystallite are produced by the slow dissolution of Zn, thus increasing the reactive surface and the utilization of the active material [10,21].

Fig. 7b shows the number of exchange electrons (NEE) per nickel atom as a function of cycle number for the Zn-doped $[Ni_4Al(OH)_{10}]OH$ samples. According to the foregoing ICP analyses, calculated molecular weights are 548, 564, 606 and 658 g mol^{-1} for the $[Ni_4Al(OH)_{10}]OH$, samples **1**, **2** and **3**, respectively. The NEE for

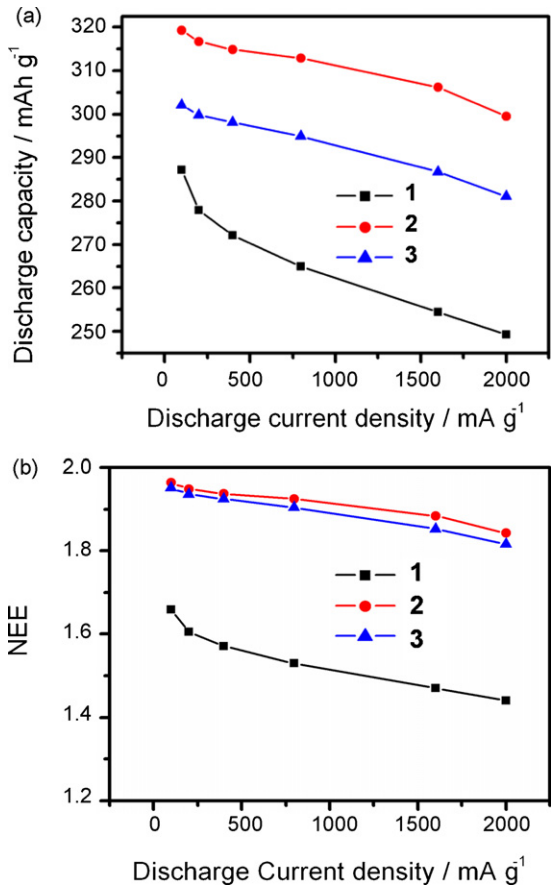

Fig. 8. (a) Gravimetric discharge capacity and (b) number of exchange electrons (NEE) as function of discharge current density for electrode with $[Ni_4Al(OH)_{10}]OH$ containing different amounts of Zn after 65 charge–discharge cycles including five activation cycles and 60 charge discharge cycles (the charge current density is 800 mA g^{-1} and the discharge current density is 400 mA g^{-1}).

each power was calculated using the formula below [27]:

$$\mathrm{NEE} = \frac{3600 C_{\mathrm{exp}}}{nF}$$

where C_{exp} is the discharge capacity in Ah g^{-1} of active material in the electrode, n is the number of moles of nickel per gram of active material, and F is Faraday's constant (96,485 C mol s^{-1}). Samples **2** and **3** have almost the same NEE (1.93) than the $[Ni_4Al(OH)_{10}]OH$ sample (1.76). It was reported that the average oxidation state of nickel in γ-phase nickel oxy-hydroxide can be up to 3.67 [43–45], and here, that of oxidized $[Ni_4Al(OH)_{10}]OH$ is 3.76, and that of Zn-doped ones can reach 3.93, which is very close to the oxidation state of Ni in NiO_2. Therefore, the existence of ZnO can make Ni be oxidized to higher oxidation state.

Fig. 8 shows the effect of discharge current density on the discharge capacity and NEE of electrode with $[Ni_4Al(OH)_{10}]OH$ containing different amounts of Zn. As it is generally observed, the discharge capacity decreases as the increase of discharge current density, however, sample **2** presents outstanding performance and has the maximal NEE (1.96) at discharge current density of 100 mA g^{-1}. It is believed that the former is caused by the diffusion of substance involved in the electrode process, because rapid movements of both electrons and reactants are needed when the electrode is discharged at high current density, any delay or resistance of the movements will certainly raise the polarization of electrode thus impairs the performance of the electrode. For the latter, it is believed that the ZnO rods existing in the active material can help the electron conductance thus makes bigger discharge capacity.

4. Conclusions

$[Ni_4Al(OH)_{10}]OH$ samples doped with different amounts of Zn were prepared by coprecipitation, subsequent hydrothermal treatment, and anion exchange reaction. XRD and SEM images show that hydrothermal treatment can make ZnO crystallize out as rods of about Ø0.7 μm × 20 μm, while the Zn-doped $[Ni_4Al(OH)_{10}]OH$ still exists in agglomerated disks of several hundreds of nanometers.

Electrochemical studies show that the ZnO rods can promote the electrochemical performance of the materials, and make the cycles more stable. ZnO rods can also make the oxidation state of Ni in Zn-doped $[Ni_4Al(OH)_{10}]OH$ be charged up to 3.93, which is very close to that in NiO_2, and the compound is still very stable.

Acknowledgements

We would like to thank The Offices of Personnel, Science and Technology (BA2006044), Jiangsu Province for financial support.

References

[1] Y. Sato, S. Takeuchi, K. Kobayakawa, J. Power Sources 93 (2001) 20.
[2] X.M. He, W.H. Pu, H.W. Cheng, C.Y. Jiang, C.R. Wan, Energy Convers. Manage. 47 (2006) 1879.
[3] X.H. Kong, X.B. Liu, Y.D. He, D.S. Zhang, X.F. Wang, Y.D. Li, Mater. Chem. Phys. 106 (2007) 375.
[4] C.C. Yang, Int. J. Hydrogen Energy 27 (2002) 1071.
[5] K. Nishio, Y. Itoh, Macromol. Symp. 156 (2000) 203.
[6] D.B. Wang, C.X. Song, Z.S. Hu, X. Fu, J. Phys. Chem. B 109 (2005) 1125.
[7] H.S. Kim, T. Itoh, M. Nishizawa, M. Mohamedi, M. Umeda, I. Uchida, Int. J. Hydrogen Energy 27 (2002) 295.
[8] X.Y. Cao, J.P. Wei, Y.J. Luo, Z.X. Zhou, Y.S. Zhang, Int. J. Hydrogen Energy 25 (2000) 643.
[9] Y.W. Tan, S. Srinivasan, K.S. Choi, J. Am. Chem. Soc. 127 (2005) 3596.
[10] C. Tessier, L. Guerlou-Demourgues, C. Faure, M. Basterreix, G. Nabias, C. Delmas, Solid State Ionics 133 (2000) 11.
[11] X.J. Han, P. Xu, C.Q. Xu, L. Zhao, Z.B. Mo, T. Liu, Electrochim. Acta 50 (2005) 2763.
[12] W.Y. Li, F.S. Cai, X.L. Gou, F. Gao, J. Chen, Acta Chim. Sin. 63 (2005) 411.
[13] W.Y. Li, S.Y. Zhang, J. Chen, J. Phys. Chem. B 109 (2005) 14025.
[14] Y.F. Zhao, Z.W. Zhu, Q.K. Zhuang, J. Solid State Electrochem. 10 (2006) 914.
[15] F. Leroux, C. Taviot-Gueho, J. Mater. Chem. 15 (2005) 3628.
[16] A.I. Khan, D. O'Hare, J. Mater. Chem. 12 (2002) 3191.
[17] L.X. Lei, W.F. Zhang, M. Hu, D. O'Hare, Chin. J. Inorg. Chem. 21 (2005) 451.
[18] C.Y. Wang, S. Zhong, D.H. Bradhurst, H.K. Liu, S.X. Dou, J. Alloys Compd. 330 (2002) 802.
[19] B. Mavis, M. Akinc, J. Power Sources 134 (2004) 308.
[20] Y.L. Zhao, J.M. Wang, H. Chen, T. Pan, J.Q. Zhang, C.N. Cao, Electrochim. Acta 50 (2004) 91.
[21] H. Chen, J.M. Wang, T. Pan, H.M. Xiao, J.Q. Zhang, C.N. Cao, Int. J. Hydrogen Energy 27 (2002) 489.
[22] M. Dixit, P.V. Kamath, J. Gopalakrishnan, J. Electrochem. Soc. 146 (1999) 79.
[23] J. Qiu, G. Villemure, J. Electroanal. Chem. 428 (1997) 165.
[24] J. Qiu, G. Villemure, J. Electroanal. Chem. 395 (1995) 159.
[25] L. Indira, M. Dixit, P.V. Kamath, J. Power Sources 52 (1994) 93.
[26] R.S. Jayashree, P.V. Kamath, J. Power Sources 107 (2002) 120.
[27] G.A. Caravaggio, C. Detellier, Z. Wronski, J. Mater. Chem. 11 (2001) 912.
[28] Y.L. Zhao, J.M. Wang, H. Chen, T. Pan, J.Q. Zhang, C.N. Cao, Int. J. Hydrogen Energy 29 (2004) 889.
[29] B. Liu, H.T. Yuan, Y.S. Zhang, Int. J. Hydrogen Energy 29 (2004) 453.
[30] L.J. Yang, X.P. Gao, Q.D. Wu, H.Y. Zhu, G.L. Pan, J. Phys. Chem. C 111 (2007) 4614.
[31] C.Y. Wang, S. Zhong, K. Konstantinov, G. Walter, H.K. Liu, Solid State Ionics 148 (2002) 503.
[32] W.K. Hu, X.P. Gao, D. Noreus, T. Burchardt, N.K. Nakstad, J. Power Sources 160 (2006) 704.
[33] W.K. Hu, D. Noreus, Chem. Mater. 15 (2003) 974.
[34] T. Pan, J.M. Wang, Y.L. Zhao, H. Chen, H.M. Xiao, J.Q. Zhang, Mater. Chem. Phys. 78 (2003) 711.
[35] R. Roto, L. Yu, G. Villemure, J. Electroanal. Chem. 587 (2006) 263.
[36] H.B. Zhang, H.S. Liu, X.J. Cao, S.J. Li, C.C. Sun, Mater. Chem. Phys. 79 (2003) 37.
[37] L.X. Lei, M. Hu, X.R. Gao, Y.M. Sun, Electrochim. Acta 54 (2008) 671.

[38] M. Hu, L.X. Lei, J. Solid State Electrochem. 11 (2007) 847.
[39] H.B. Liu, L. Xiang, Y. Jin, Cryst. Growth Des. 6 (2006) 283.
[40] J. Chen, W. Lei, W.Q. Chai, Z.C. Zhang, C. Li, X.B. Zhang, Solid-State Electron. 52 (2008) 294.
[41] S. Ohara, T. Mousavand, M. Umetsu, S. Takami, T. Adschiri, Y. Kuroki, M. Takata, Solid State Ionics 172 (2004) 261.
[42] M. Tanaka, M. Nishikino, H. Yamatani, K. Nagashima, T. Kimura, Y. Furukawa, H. Murakami, S. Saito, N. Sarukura, H. Nishimura, K. Mima, Y. Kagamitani, D. Ehrentraut, T. Fukuda, Appl. Phys. Lett. 91 (2007) 231117.
[43] C. Faure, C. Delmas, M. Fouassier, J. Power Sources 35 (1991) 279.
[44] D.A. Corrigan, S.L. Knight, J. Electrochem. Soc. 136 (1989) 613.
[45] R. Barnard, C.F. Randell, F.L. Tye, J. Appl. Electrochem. 10 (1980) 109.